RSC Advances

REVIEW

View Article Online
View Journal | View Issue

Cite this: *RSC Adv.*, 2014, **4**, 118

Progress in La-doped $SrTiO_3$ (LST)-based anode materials for solid oxide fuel cells

Xinwen Zhou, Ning Yan, Karl T. Chuang and Jingli Luo*

Received 30th May 2013
Accepted 25th October 2013

DOI: 10.1039/c3ra42666a

www.rsc.org/advances

Solid oxide fuel cells (SOFCs) have appeared as a promising technology for a wide variety of potential commercial applications to lessen the urgency of energy shortage and environmental pollution associated with using conventional fossil fuels. Among the worldwide SOFCs research activities, the progress of SOFCs fed with hydrocarbon fuels that contain trace amount of H_2S is one of the most important research directions. Thereby, it becomes crucial to design novel electrode materials with enhanced catalytic activity, stability and tolerances to carbon deposition and sulfur poisoning. La-substituted $SrTiO_3$ (LST) based perovskite anodes have been widely investigated because of their high electronic conductivity in reducing atmospheres, excellent dimensional and chemical stability upon redox cycling and outstanding sulfur and coking tolerances. In this review paper, we will describe the development of LST-based anode materials for SOFCs in recent years. The synthesis, structure and fuel cell performance of the doped LST and LST-based composite anode materials are summarized in detail. The mechanism of H_2S-induced enhancement effect for electrochemical reactions on the LST-based anode materials is explored. The challenges related to the future developments of LST-based anode materials for SOFCs are also discussed.

1. Introduction

Conventional fossil fuels are the main energy sources at present and for the foreseeable future. However, the energy sources of this type are limited in nature and non-renewable, which can lead to serious energy crises in the future. Also, the environmental problems associated with using conventional fossil fuels are causing public concerns and frequently appear as the headlines in various social media. Solid oxide fuel cells (SOFCs), on the other hand, have been considered as one of the most efficient and environmental-friendly technologies to tackle some of challenges that energy industry is currently facing. The distinguishing advantages of SOFCs include high energy conversion efficiency which is projected to be up to 60%[1] and great fuel flexibility. In theory, SOFCs can be fueled by essentially any fuels ranging from gaseous hydrogen, hydrocarbons to solid carbon. A typical SOFC single cell is consisted of three major components: a cathode, an anode and a ceramic electrolyte which is usually a solid oxygen ionic conductor. On the cathode side, O_2 is reduced and incorporated into the electrolyte defects, namely oxygen vacancies, resulting in the formation of O^{2-} ions. These O^{2-} ions will be driven by the difference of chemical potential, which is established between the two opposite electrodes, to move through the electrolyte to the anode where they can oxidize the fuels. All the electrons generated during the electrochemical oxidation process will be released to the external circuit for power generation.

Presently, one of the major concerns associated with utilizing hydrocarbon fuels in SOFCs is the anode catalyst coking and sulfur poisoning since H_2S exists in most raw feedstock. The commonly employed Ni-based anode catalyst can be easily deactivated by carbon deposits and suffers irreversible sulfur poisoning. Although steam reforming and desulfurization enable the suppression of coking and H_2S removal, these processes inevitably add the extra cost and complexity into the overall system. Therefore, intensive efforts have been devoted to developing novel anode catalysts.

In recent years, many excellent review papers have been published with focusing on cathodes,[2–4] electrolytes,[5–8] interconnects,[9,10] sealants,[11,12] current collector materials,[13,14] SOFCs models[15,16] and other correlative studies[17,18] about SOFCs. Also, a number of excellent review papers are available in the literature summarizing the progress of SOFCs anode catalysts.[19–21] Thus, in this review, first, we will only very briefly introduce the commonly used anode materials for SOFCs. Then, we will focus on the recent progress of La-substituted $SrTiO_3$ (LST) based anode materials since the doped $SrTiO_3$ has attracted increasing attentions as a promising anode candidate. The development of a variety of LST-based anode materials will be reviewed in details. Finally, the phenomena and mechanisms of the H_2S-induced enhancement of the SOFC performance in SOFCs fed by H_2S containing fuels will be summarized *via* using the

Department of Chemical and Materials Engineering, University of Alberta, Edmonton, Alberta, Canada T6G 2G6. E-mail: Luoj@ualberta.ca; Fax: +1 780 492 2881; Tel: +1 780 492 2232

LST-based anode. Meanwhile, the LST-based anode fabrication process, the relationship between microstructure and the fuel cell performance, and miscellaneous issues regarding to LST-based materials will also be discussed. A complete and comprehensive coverage of all the research activities on the LST-based anode materials may not be an easy task, therefore, this short review paper is meant to be a summary of most of the correlative research in recent years.

2. A brief overview of common anode materials for SOFCs

As described in the earlier review articles,[2,20,21] the general requirements for SOFCs anode materials should include: high electronic conductivity, excellent catalytic activity towards electro-oxidation of fuels, high ionic conductivity, chemical and thermal stability, adequate durability and compatibility with other SOFCs components, easy fabrication, and low cost. The other desirable properties are tolerances to carbon deposition or coking when using hydrocarbon fuels,[22] and to sulfur poisoning when using fuels containing H_2S.[23,24]

In general, the anode materials in SOFCs can be categorized as metal-based cermet, simple oxides, complex oxides and other alternative anode materials.

Advantages of the metal-based anode materials (*e.g.* Ni–yttria-stabilized-zirconia (Ni–YSZ)) include most requirements for anode materials mentioned earlier. However, the metal-based anode materials are easily poisoned by the trace impurities (*e.g.* H_2S) in fuels, which could lead to serious fuel cell performance degradation. It has been revealed that Ni/YSZ anode supported SOFCs can only tolerate up to 1 ppm H_2S and 10 ppm HCl without significant performance degradation.[25] Carbon deposition, redox cycling instability and Ni agglomeration upon prolonged usage are the other major problems observed on Ni/YSZ anode. Recently, Ni and Cu-based cermet anode catalysts have been reviewed.[20,21,24,26] Some metal-based anode materials such as $Ir/Ce_{0.9}Gd_{0.1}O_{2-\delta}$,[27] $Ni–Gd_{0.1}Ce_{0.9}O_{2-\delta}$[28,29] have been reported. Zirconia-based (*e.g.* $Y_{0.2}Ti_{0.18}Zr_{0.62}O_{1.90}$[30]) and ceria-based (*e.g.* CeO_2,[31] $Ce_{0.8}Gd_{0.2}O_{1.9}$[32]) fluorites are the common simple oxide anode materials and have been reviewed particularly.[20,21,33]

Perovskite-based oxide (general stoichiometry ABO_3, where A and B are metal cations) is a typical complex oxide catalyst which is known to have excellent thermal and mechanical stability, physical compatibility with typical electrolyte materials, flexibility, and low production cost, which makes it attractive as electrode material in SOFCs. Recently, different perovskite-based materials including chromite (*e.g.* $La_{0.75}Ba_xSr_{0.25-x}Cr_{0.5}Mn_{0.5}O_3$[34]), vanadate (*e.g.* $La_{0.7}Sr_{0.3}VO_{3.85}$[35]), titanate (*e.g.* $Sr_{0.895}Y_{0.07}TiO_{3-\delta}$,[36] Nb-doped $SrTiO_3$[37]) *etc.* have been reported to be used as electrode materials in SOFCs. Double perovskites $A_2BB'O_6$ containing alternating $BO_{6/2}$ and $B'O_{6/2}$ corner-shared octahedral[38] are the first on the list of interest due to their reasonable ionic conductivity, redox stability and stability in presence of sulphurous impurities.[39,40] Some new double perovskites such as $LnBaCo_{1.6}Ni_{0.4}O_{5+\delta}$ (Ln = Pr, Nd, and Sm).[41] Sr_2MMoO_6 (M = Mg, Mn),[42] $Sr_{2-x}VMoO_{6-\delta}$,[43] La_2ZnMnO_6[44] have been explored as electrode materials in SOFCs. Different perovskite-based anode materials applied for SOFCs have been reviewed.[20,21,45–47] In addition, other type of complex oxides such as rutile,[48] tungsten bronze,[49] *etc.* are also explored as anode catalysts.[20,21]

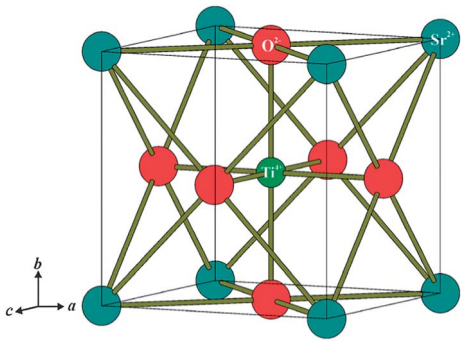

Fig. 1 Idealized structure of cubic perovskite $SrTiO_3$. Reprinted from ref. 50, Copyright (2013), with permission from Royal Society of Chemistry.

For perovskite-based materials ABO_3, varying A and/or B can generate a large number of different compounds. Among them, strontium titanate ($SrTiO_3$) whose A and B-sites are occupied by divalent Sr^{2+} and tetravalent Ti^{4+} (Fig. 1)[50] is an excellent example to explain the origin of the increased electronic conductivity upon doping. O-2p orbitals and the empty conduction band from Ti-3d orbitals make the electronic energy band of $SrTiO_3$ exhibit an n-type semiconducting behavior in reducing atmospheres due to the redox couple Ti^{4+}/Ti^{3+}.[51] An A-site or a B-site doped $SrTiO_3$ can improve its total electrical conductivity. Lanthanum is an appropriate donor dopant because its ionic radius is similar to that of Sr^{2+}. Its stability in the trivalent state ensures its incorporation into the perovskite lattice as La^{3+}. Due to the difference in valence between La^{3+} and Sr^{2+}, introduction of La into the lattice requires that the lattice defect structure be modified to maintain electroneutrality.[52] At the same time, the introduction of La to Sr sites causes the formation of oxygen-rich planes, which will improve the ionic conductivity of LST.[20] La-substituted $SrTiO_3$ (LST) based anode materials have been widely investigated because of their high electronic conductivity in reducing atmospheres, outstanding dimensional and chemical stability upon redox cycling and excellent sulfur and coking tolerances.

3. LST-based anode materials

This section reviews the synthesis, structure, thermal and electrical properties, and fuel cell performance of LST-based candidates including LST, further doped LST and LST composite anode materials.

3.1 $La_xSr_{1-x}TiO_3$

It is well known that LST materials sintered in reducing atmospheres cause a change in the titanium valence from Ti^{4+} to Ti^{3+},

thus enhancing the electronic charge carrier concentration.[51] Moos *et al.*[53] investigated the solubility of lanthanum in $La_xSr_{1-x}TiO_3$ in oxygen-rich atmospheres. A pure strontium vacancy compensation mechanism was observed for lanthanum contents up to $x = 0.3$. Above $x = 0.4$, additional titanium vacancies form, but their concentration remains negligible compared to the predominating strontium vacancies. At $x = 0.5$ and 0.6 the lattice structure was found to be slightly distorted.

LST-based materials used as potential anode for SOFCs were firstly investigated by Irvine *et al.*[54] in 1997. They found that single phase A-site deficient perovskites $La_xSr_{1-3x/2}TiO_{3-\delta}$ could be achieved in air at $0 \leq x \leq 0.6$, and the materials remained at single phase under both high and low oxygen partial pressures at 930 °C. As La content increased, the electrical conductivity also increased to as high as 7 S cm^{-1} ($P_{O_2} = 10^{-20}$ atm) at 930 °C for $x = 0.6$. This kind of A-site deficient LST-based anode materials was further studied by the group.[55–57] New family of perovskite oxides such as $La_2Sr_{n-2}Ti_nO_{3n+1}$[58,59] and $La_4Sr_{n-4}Ti_nO_{3n+2}$[60] were also explored as a potential anodes for fuel cells. Due to the high electrical conductivity, LST-based materials were also used as the interconnect materials[61] and support layer[62] for resisting carbon deposition.

The thermal, electrical, and electrocatalytical properties of LST powders ($La_xSr_{1-x}TiO_3$, $x = 0.1$, 0.2, 0.3, 0.35, and 0.4) were studied by Marina *et al.*[52] The samples sintered in air exhibited an electrical conductivity in the order of 1–16 S cm^{-1}. But $La_xSr_{1-x}TiO_3$ sintered in hydrogen at 1650 °C showed 80–360 S cm^{-1} under the typical SOFCs experimental operation conditions. No significant chemical expansion or contraction of $La_xSr_{1-x}TiO_3$ with $x < 0.4$ was observed when exposed under a wide range of P_{O_2} because the thermal expansion of LST was close to that of YSZ. $La_xSr_{1-x}TiO_3$ was found to be dimensionally and chemically stable when subjected to oxidation–reduction cycling. The structural and electrical properties of $La_{0.3}Sr_{0.7}TiO_{3-\alpha}$ and other donor-doped $SrTiO_3$ based oxides were also investigated by Hashimoto *et al.*[63,64] They found that the conductivity showed a strong dependence on the P_{O_2}. When the P_{O_2} was over 100 Pa, the conductivity drastically dropped with increasing P_{O_2}. The $La_{1-x}Sr_xTiO_3$ ($x = 0.5$, 0.6, 0.7, 0.8) samples have been tested for possible use as a matrix phase for producing composite anodes for SOFCs.[65] It was found that $La_{0.5}Sr_{0.5}TiO_3$ demonstrated some ionic conductivity and could be used as a basic phase for producing composite anodes. The thermal expansion mechanism of $La_xSr_{1-x}TiO_3$,[66] sintering characteristics of $(La_xSr_{1-x})_{1-y}Ti_{1-z}O_3$[67] and $La_xSr_{1-x}TiO_3$[68] were also studied.

A series of A-site deficient perovskite oxides $(La_{0.3}Sr_{0.7})_{1-x}TiO_{3-\delta}$ ($x = 0$, 0.03, 0.05, 0.07, 0.10) were investigated by Li *et al.*[69] Standard four terminal DC methods and electron-blocking method were applied to measure the total electrical conductivity and ionic conductivity, respectively. As A-site deficiency level increased, the ionic conductivity increased but the electronic conductivity decreased (Fig. 2). The ionic conductivity of $(La_{0.3}Sr_{0.7})_{0.93}TiO_{3-\delta}$ was as high as 0.2–1.6 $\times 10^{-2}$ S cm^{-1} at 500–950 °C and 1.0 $\times 10^{-2}$ S cm^{-1} at 800 °C, more than twice that of $La_{0.3}Sr_{0.7}TiO_{3-\delta}$. Its electrical conductivity was in the range of 83–299 S cm^{-1} at 50–950 °C and 145 S cm^{-1} at 800 °C. It was also assumed that A-site deficiency could improve the thermal stability of $(La_{0.3}Sr_{0.7})_{1-x}TiO_{3-\delta}$. Burnat *et al.*[70] found that the phase stability of A-site deficient $La_{0.2}Sr_{0.7}TiO_3$ could be enhanced significantly by adding some Sr to form $La_{0.2}Sr_{0.706}TiO_3$. The secondary phase such as TiO_2 could invoke the loss of electrical performance.

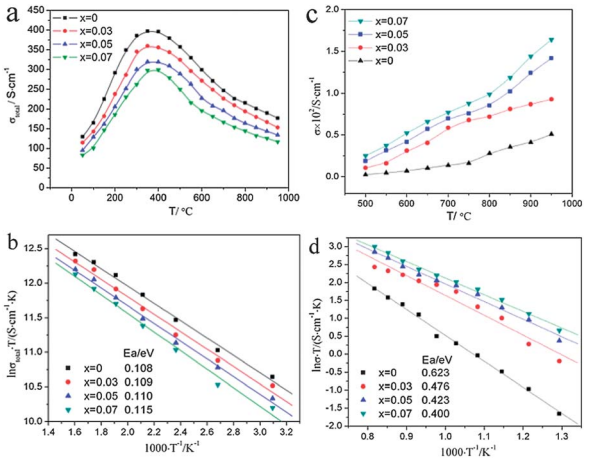

Fig. 2 Electrical conductivities of $(La_{0.3}Sr_{0.7})_{1-x}TiO_{3-\delta}$ ($x = 0$, 0.03, 0.05, 0.07, 0.10) as functions of A-site-deficient level and temperature in 50–950 °C (a) and ln σT *versus* 1000/T in 50–350 °C (b). Ionic conductivities of $(La_{0.3}Sr_{0.7})_{1-x}TiO_{3-\delta}$ ($x = 0$, 0.03, 0.05, 0.07, 0.10) as functions of A-site-deficient level and temperature (c) and ln σT *versus* 1000/T (d) in 500–950 °C. Reprinted from ref. 69, Copyright (2010), with permission from International Association for Hydrogen Energy.

The performances of fuel cells were compared using LST anode with that using Y doped $SrTiO_3$ (YST).[71] It was found that adding the extra electrolyte materials, such as YSZ, into the doped $SrTiO_3$ anode could improve cell performance, suggesting insufficient ionic conductivity of LST. Moreover, the electrical conductivity of YST was lower than that of LST at the same temperature. Recently, A-site deficient $Y_{0.07}Sr_{0.895}TiO_3$ (YST) and $La_{0.2}Sr_{0.7}TiO_3$ (LST) were synthesized through spray pyrolysis method and compared for the electrical conductivity and chemical expansion.[72] Under same reducing conditions, YST had better chemical expansion, while LST had better conductivity. To accommodate both conductivity and redox stability, LST was sintered at 1400 °C in air and reduced at around 1000–1200 °C, they then became suitable candidates for full ceramic based SOFCs anodes. Computational prediction was also explored to study the properties of LST-based materials.[73]

Under the operating conditions of SOFCs, the chemical compatibility between the electrode materials and the electrolyte was a major concern. Burnat *et al.*[74] investigated the chemical interactions between common electrolyte materials and 20 wt% La doped Sr titanates with various A-site occupancy by SEM/EDX microscopy and XRD. It was found that all A-site deficient LSTs promoted a reaction with Sc and YSZ, while stoichiometric LST was more stable.

From the above analysis, we can conclude the following. The maximal solubility of La in $SrTiO_3$ is 0.6. However, the common x in $La_xSr_{1-x}TiO_3$ is 0.3 or 0.4. The structure will be distorted when the x exceeds 0.5. La-doped LST materials with a normal

stoichiometry and A-site deficiency are the two main candidates having been examined. Compared to the stoichiometric LST, A-site deficient LST has higher conductivity but lower phase stability and chemical stability.

3.2 Doped $La_xSr_{1-x}TiO_3$

The main disadvantages of LST anode materials are their low ionic conductivity and poor electrocatalytic activity. Presently, the two main methods of increasing the ionic conductivity and improving the fuel cell performance including doping LST with other metal ions and introducing of active second phase to LST to form composite anode.

3.2.1 A-site doped LST. Cerium-based compounds were particularly interesting since these materials were known to be highly active towards the direct oxidation of fuels. Périllat-Merceroz *et al.*[75] investigated the possibility of improving the catalytic and electrocatalytic properties of $La_{0.33}Sr_{0.67}TiO_{3+\delta}$ materials by introducing the Ce^{4+}/Ce^{3+} redox couple through partial substitution of La by Ce in the structure of the $x = 0.33$ member of the $La_xSr_{1-x}TiO_{3+\delta}$ series. The pure phase of $La_{0.33}Sr_{0.67}TiO_{3+\delta}$ (LST) and $La_{0.23}Ce_{0.1}Sr_{0.67}TiO_{3+\delta}$ (LCST) were synthesized through Pechini route in reducing atmosphere. Sintering the LCST in oxidizing and reducing atmosphere at different temperatures could ensure the presence of nanoparticles of active Ce-rich phase (Fig. 3a) within LST network and then enhance their activity towards CH_4 oxidation. The catalytic tests in methane steam reforming at 900 °C (CH_4–H_2O = 10/1) showed that the properties of the Ce-rich phase within LST network (LCST-ox) are greatly improved compared with pure LST and LSCT materials (Fig. 3b). More importantly, this material maintained a high resistance to the carbon deposition. It was then considered that the LCST materials of this kind would be a promising anode material for SOFCs directly operating on slightly wet CH_4.

Vincent *et al.*[76] found that Ba partial substitution for Sr in LST ($La_{0.4}Sr_{0.6-x}Ba_xTiO_3$, $0 < x \leq 0.2$ (LSBT)) could increase its ionic conductivity, catalytic activity to the oxidation of CH_4 and improve the stability of the LST structure. Fuel cells were fabricated using commercial YSZ disks (300 μm thick and 25 mm in diameter) as the electrolyte and the composited YSZ/LSM 50/50 wt% as the cathode. It was observed that all fuel cells using LST or LSBT had limited activity for the conversion of hydrogen and methane, and the activity increased with the level of substitution by Ba. Most importantly, the fuel cell performance was significantly enhanced when H_2S was present in either CH_4 or H_2 fuel. The different amount of $La_{0.4}Sr_{0.5}Ba_{0.1}TiO_3$ was impregnated into porous YSZ by Vincent *et al.*[77] Fig. 4 compares the performance with the number of times LSBT was impregnated into porous YSZ. The temperature for each test was 850 °C and the sequences of the fuels used were: H_2, H_2 + 0.5% H_2S, CH_4 + 0.5% H_2S and CH_4. The experiments clearly suggested that when the feed was CH_4 + 0.5% H_2S, the power density was consistently higher than that in pure H_2 and pure CH_4. Six impregnations provided maximum power density in all the fuels. The maximum power density was 84 mW cm^{-2} when the feed was CH_4 + 0.5% H_2S, which was about 3.5 times of that when using pure CH_4 as the fuel. Based on the Ba-doped LST materials, Li *et al.*[78] found that pure $BaTiO_3$ anode had higher tolerance to carbon deposition, better electrochemical performance and much higher stability during long term operation compared to $SrTiO_3$ and $La_2Ti_2O_7$ anodes, especially in H_2S-containing atmospheres.

In addition to the Ba-doping in Sr site, LST with Ca-doping in Sr site was also studied by Verbraeken *et al.*[79] The pure $La_{0.20}Sr_{0.25}Ca_{0.45}TiO_3$ (LSCT) anode initially showed a poor performance. Then the LSCT was impregnated with ceria and nickel oxide to form different anode materials including pure LSCT, LSCT + 10 wt% CeO_2, LSCT + 5 wt% Ni, LSCT + 10 wt% CeO_2 + 5 wt% Ni, LSCT + 8 wt% CeO_2 + 3 wt% Ni. When both nickel and ceria were added as impregnates, a drastic

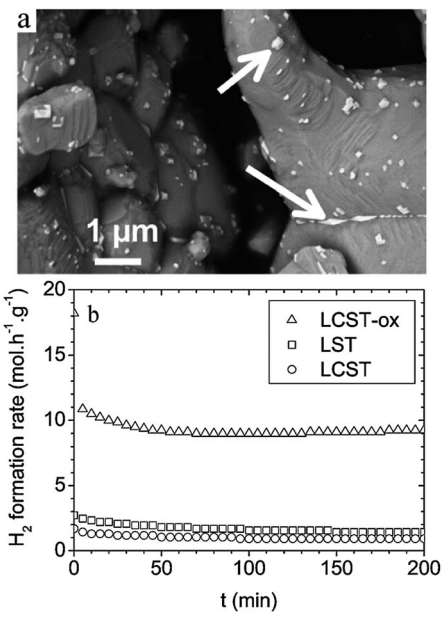

Fig. 3 (a) FEG-SEM image of LCST after oxidation at 1200 °C in air. The arrows point at Ce-enriched phases. (b) Hydrogen formation rates *vs.* time upon reaction of a 10 : 1 : 9 CH_4–H_2O–N_2 mixtures over LST, LCST and LCST-ox samples. T = 900 °C. Reprinted from ref. 75, Copyright (2011), with permission from American Chemical Society.

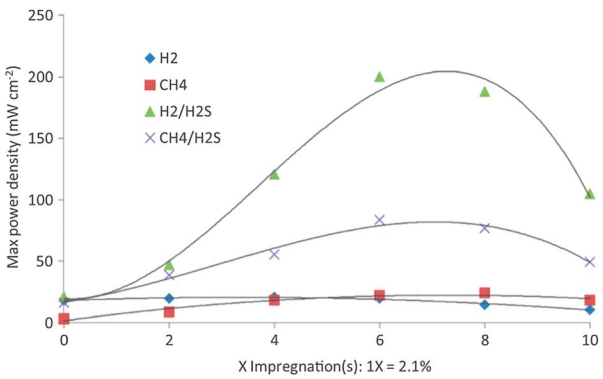

Fig. 4 Dependence of compensated maximum power density on the number of times LSBT was impregnated into YSZ obtained at 850 °C. Reprinted from ref. 77, Copyright (2012), with permission from Elsevier.

improvement of the anode performance was observed comparing to cases of impregnating with ceria only and pure LSCT. These new anodes also showed excellent stability upon redox cycling, and appeared as a promising alternative to Ni–cermet electrodes. Further studies were done on the structure and conductivity of a series of Ca-doping in A-site deficient perovskite $La_{0.2}Sr_{0.7-x}Ca_xTiO_3$.[80] The results indicated that $La_{0.2}Sr_{0.7-x}Ca_xTiO_3$ with $0.1 \leq x \leq 0.4$ were tetragonal and samples with $0.45 \leq x \leq 0.7$ were orthorhombic at room temperature. A 0.3% increase in lattice volume of the samples was observed after their reduction at 900 °C in 5% H_2. The conductivity was definitely improved when compared to $La_{0.2}Sr_{0.7}TiO_3$. By increasing Ca doping content, the conductivity of the reduced samples increased dramatically, reaching the peak of 27.53 S cm^{-1} in $La_{0.2}Sr_{0.25}Ca_{0.45}TiO_3$. However, the conductivity decreased as x was further increased. Later, a solution method was introduced to synthesize $La_{0.25}Sr_{0.25}Ca_{0.45}TiO_3$ by Yaqub *et al.*[81]

3.2.2 B-site doped LST. In relation to A-site doping, the majority of the research activities were concentrated on the B-site substitution. LST-based materials doped with various transition metal elements (Cr, Mn, Fe, Co, Ni, Co, Ga, Al, Mg, Sc and Nb *etc.*) in B-site have been investigated in recent years.

The $La_{0.7}Sr_{0.3}Cr_{0.8}Ti_{0.2}O_{3-\delta}$ with chromium-rich composition was synthesized using the Pechini method[82] and showed a n-type conductivity and high stability under reducing conditions. The perovskite electrodes were electrochemically active towards hydrogen oxidation, although the electronic conductivity (0.1 S cm^{-1} at 850 °C and 10^{-20} bar P_{O_2}) was not sufficient. A series of perovskite oxides $La_{0.75}Sr_{0.25}Cr_{0.5}X_{0.5}O_{3-\delta}$ (X = Co, Fe, Ti, Mn) as SOFCs anode electrocatalysts have been studied by Danilovic *et al.*[83] They concluded that the performance of the perovskite oxides depended on the nature of the substituent element X. Temperature programmed reaction (TPR) of CH_4 under O_2-free conditions showed that the catalytic activity of the oxides for conversion of CH_4 was in the order of Co > Mn > Fe > Ti. Within this series of catalysts, the order of maximum fuel cell power density depended on feed: CH_4, X = Fe > Mn > Ti; H_2, X = Fe > Mn > Ti; and 0.5% H_2S/CH_4, X = Ti > Fe > Mn. It was also found that gadolinia doped ceria (GDC) or YSZ combined with $La_{0.75}Sr_{0.25}Cr_{0.5}Ti_{0.5}O_{3-\delta}$ could improve the performance. The $La_{0.3}Sr_{0.55}Ti_{1-x}Cr_xO_{3-\delta}$ single-phase perovskite structure can be obtained in air when the dopant content of Cr did not exceed 20 mol%.[84] The particle diameter obtained at 800 °C was less than 60 nm and the particles showed an excellent chemical compatibility with YSZ at 1400 °C. At 800 °C, the conductivity of $La_{0.3}Sr_{0.55}Ti_{0.8}Cr_{0.2}O_{3-\delta}$ pellet was 1.96×10^{-3} S cm^{-1} in static air, which needed to be further improved. The Cr-doping decreased the lattice parameter while it increased the sinterability of $La_{0.3}Sr_{0.7}Ti_{1-x}Cr_xO_{3-\delta}$ (LSTC, $x = 0, 0.1, 0.2$) materials.[85] The total electrical conductivity decreased as Ti cations were partially substituted by Cr. However, the electrical conductivity of the LSTC sample with $x = 0.2$ was still 53 S cm^{-1} at 800 °C in 5% H_2/Ar. The electrical conductivity of Cr-doped samples declined significantly when the testing atmosphere shifted from 5% H_2/Ar to air. When the atmosphere was switched back to 5% H_2/Ar, the values of the electrical conductivity could mostly be recovered except for the initial cycle. The highest power density obtained with $La_{0.3}Sr_{0.7}Ti_{0.8}Cr_{0.3}O_{3-\delta}$ as the anode reached 43.86 mW cm^{-2} at 900 °C using H_2 as the fuel, which was higher than that of undoped $La_{0.3}Sr_{0.7}TiO_{3-\delta}$ anode material (~30 mW cm^{-2}). The better fuel cell performance of LSTC anode materials could be attributed to the better contact between LSTC and YSZ, and the increased electrical conductivity.

The microstructural and electrochemical properties of Mn-doped LST anode material $La_{0.4}Sr_{0.6}Ti_{0.8}Mn_{0.2}O_{3\pm\delta}$ (LSTM) fabricated *via* liquid-phase impregnation have also been investigated.[86] The thermal stability was improved with decreasing Mn content. The electrical conductivity of a 10 wt% CeO_2–50 wt% LSTM–YSZ composite anode was higher than that of a 50 wt% LSTM–YSZ anode and was stable under reducing conditions. The maximal power densities of 50 wt% LSTM–YSZ anode were less than 100 mW cm^{-2} over the entire measured temperature range. The addition of 10 wt% of CeO_2 and 1 wt% of Pd as catalysts increased the power density in H_2 to 150 and 210 mW cm^{-2} at 800 and 850 °C, respectively. The performance of A-site-deficient $(La_{1-x}Sr_x)_{0.95}Mn_{0.5}Ti_{0.5}O_{3-\delta}$ and A-site-stoichiometric $La_{1-x}Sr_xMn_{0.5}Ti_{0.5}O_{3-\delta}$ perovskites were studied by Kolotygin *et al.*[87] The total conductivity, thermal and chemical expansion, and steady-state oxygen permeation limited by oxygen surface exchange kinetics increased with increasing x. The presence of H_2S traces (5 ppm) in H_2-containing gas mixtures did not result in detectable decomposition of the perovskite phases. $La_{0.6}Sr_{0.4}Ti_{1-x}Mn_xO_{3-\delta}$ (LSTM, $x = 0.2, 0.4, 0.6, 0.8$) were also studied.[88] The increase in electrical conductivity as well as oxygen vacancy concentration in a reducing atmosphere resulted in an increase in the higher H_2 and CH_4 oxidation rate in SOFCs. The single cell with a $La_{0.6}Sr_{0.4}Ti_{0.2}Mn_{0.8}O_{3-\delta}$ anode, $Ba_{0.6}Sr_{0.4}Co_{0.5}Fe_{0.5}O_{3-\delta}$–GDC cathode and GDC electrolyte reached maximum power densities of 0.29 W cm^{-2} and 0.24 W cm^{-2} in humidified H_2 and CH_4 at 800 °C, respectively. The recent study on the electrochemical and thermomechanical properties of $La_{0.5}Sr_{0.5}Mn_{0.5}Ti_{0.5}O_{3-\delta}$ and $(La_{0.55}Sr_{0.45})_{0.95}Mn_{0.5}Cr_{0.3}Ti_{0.2}O_{3-\delta}$[89] confirmed the suitability of LSTM as an alternative anode material.

The ionic transference numbers of $La_{0.4}Sr_{0.5}Ti_{0.6}Fe_{0.4}O_{3-\delta}$ were determined to be between 2×10^{-4} to 6×10^{-4} in air by faradaic efficiency measurements, indicating that the substitution of Sr for La would reduce the ionic and total conductivity.[90] Nonetheless the La containing compositions showed sufficient stability and a matched thermal expansion coefficient with YSZ. A series of candidate dopants X (X = Al^{3+}, Ga^{3+}, Fe^{n+}, Mg^{2+}, Mn^{n+} and Sc^{3+}) have been investigated in their search for $La_{0.33}Sr_{0.67}Ti_{0.92}X_{0.08}O_{3+\delta}$ anodes by Miller *et al.*[91] The impedance results for the electrical half cell tests in H_2–3% H_2O at 900 °C are shown in Fig. 5a. The $La_{0.33}Sr_{0.67}TiO_{3+\delta}$ had the lowest polarisation resistances; doped Sc and Ga gave had the second lowest polarisation resistances followed by doped Al, Fe, Mn and Mg. Fig. 5b shows the over-potential *versus* current density curves corresponding to the $La_{0.33}Sr_{0.67}Ti_{0.92}X_{0.08}O_{3+\delta}$–YSZ anodes. A reduction in polarisation resistance was observed when the anode was under the load compared to that at the open circuit potential. Ti site Fe doped LST was also explored as solid oxide electrolysis cells (SOECs) cathodes for hydrogen production.[92]

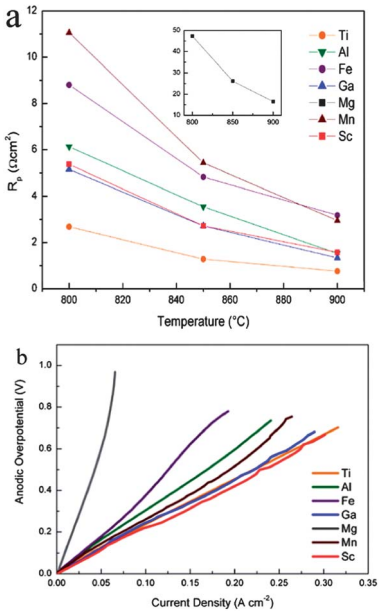

Fig. 5 (a) The variation of polarization resistance with temperature for all LSTX–YSZ anodes. (b) Anodic overpotentials of $La_4Sr_8Ti_{11}XO_{36+\varepsilon}$–YSZ anodes operating in H_2–3% H_2O at 900 °C. Reprinted from ref. 91, Copyright (2011), with permission from Elsevier.

It is well known that catalytic activities of transition metals generally follow the order of Co > Mn > Ni > Fe > Cr on the oxidation–reduction process.[93] Thus, various amount of Co was doped into Ti-site in $La_{0.2}Sr_{0.8}TiO_3$ (LSTC) by Yoo *et al.*[94] The stability of LST anode was greatly improved with the Co doping. A single cell with Ni-impregnated LSTC–GDC composite as the anode, $Ba_{0.5}Sr_{0.5}Co_{0.8}Fe_{0.2}O_{3-\delta}$ (BSCF) as the cathode and $La_{0.9}Sr_{0.1}Ga_{0.8}Mg_{0.2}O_{3-\delta}$ (LSGM) as the electrolyte exhibited a maximum power density of ~250 mW cm^{-2} at 800 °C. The R_p value of anode (~0.9 Ω cm^2) was responsible for most of the total R_p value (~0.95 Ω cm^2). Li *et al.*[95] also considered LSTC as a promising anode candidate and found that at 1500 °C, the solid solution limits of La in $La_xSr_{1-x}TiO_{3-\delta}$ and Co in $La_{0.3}Sr_{0.7}Co_yTi_{1-y}O_{3-\delta}$ were about 40 mol% and 7 mol%, respectively. Co-doping into $La_{0.3}Sr_{0.7}TiO_{3-\delta}$ increased the oxygen vacancy concentration and decreased the migration energy for oxygen ions, leading to a significant increase in ionic conductivity but at the expense of some electrical conductivity loss. The electrical and ionic conductivities of $La_{0.3}Sr_{0.7}Co_{0.07}Ti_{0.93}O_{3-\delta}$ at 700 °C were 63 S cm^{-1} and 6×10^{-3} S cm^{-1} respectively. At the same time, both $La_{0.3}Sr_{0.7}TiO_{3-\delta}$ and $La_{0.3}Sr_{0.7}Co_{0.07}Ti_{0.93}O_{3-\delta}$ showed relatively stable electrical conductivities under oxygen partial pressure of 10^{-14} to 10^{-19} atm at 800 °C. Recently, Cui *et al.*[96] found that the doped Co in $La_{0.3}Sr_{0.7}Co_{0.07}Ti_{0.93}O_{3-\delta}$ could exsoluted to the LSCT surface after reduction in H_2 at 900 °C. The active Co nanoparticles could reduce the anode polarization resistance. A maximum power density of 300 mW cm^{-2} was achieved when the cell was fueled with H_2 containing 5000 ppm H_2S at 900 °C. Also, the LSCT exhibited high sulfur resistance and redox stability. The performance of $La_{0.2}Sr_{0.8}Ti_{0.98}Co_{0.02}O_3$ anode material was reported by Yoo *et al.*[97] The maximum power density of the cell with Ni-impregnated LSTC–GDC anode increased from 638 to 924 mW cm^{-2} at 800 °C for 30 h in H_2. This value was very high compared to other reported values using LSTC anode. In CH_4 fuel, while the cell performance with Ni–GDC anode decreased ~44% for 30 h, the cell performance with Ni-impregnated LSTC–GDC anode was relatively stable for 30 h. The study further proved that LST anode exhibited high tolerance to carbon induced deactivation in the internal utilization of hydrocarbon fuels while sustained a reasonable performance in H_2 fuel compared to the conventional Ni-based anode. The reproducibility of crystallographic information of $La_{0.4}Sr_{0.6}Ti_{1-x}Co_xO_{3+\delta}$ $(0.0 \leq y \leq 0.5)$ was also studied by XRD and TEM techniques.[98]

A new $La_{0.5}Sr_{0.5}Ti_{0.75}Ni_{0.25}O_{3-\delta}$ (LSTN) compound was synthesized using a nitrate–citrate gel technique.[99] The LSTN presented a metallic behavior after reduction at 1200 °C in H_2. The high-temperature treatment led to the precipitation of Ni nanoparticles on the surface and an improved electrical conductivity that may be due to the formation of excess Ti^{3+}. The obtained polarization resistance was 0.55 Ω cm^2 at 800 °C under H_2–H_2O (97/3) using symmetrical cells.

Ruiz-Morales *et al.*[100] has demonstrated the concept of inducing functionality through disorder of extended defects in LST. Mn was known to accept lower coordination numbers in perovskites and thus it may facilitate oxide-ion migration. Similarly Ga was well known to adopt lower coordination than octahedral in perovskite-related oxides. They further studied the Ga and Mn doped in Ti site for $La_4Sr_8Ti_{12}O_{38-z}$. The maximum power density in wet H_2 was close to 0.5 W cm^{-2} and the power density in wet CH_4 was two times higher than that in 5% H_2, reaching the value of about 0.35 W cm^{-2}. After running for two days, cycling from 950 °C to 850 °C, in wet 5% H_2, wet H_2 and wet methane, no trace of carbon could be detected visually or by thermogravimetric analysis. It was thought that the materials design concept could lead to the devices that enable more-efficient energy extraction from fossil fuels and carbon-neutral fuels. Based on the research of the $La_{0.33}Sr_{0.67}Ti_{0.92}X_{0.08}O_{3+\delta}$,[91] $La_{0.4}Sr_{0.4}Ga_xTi_{1-x}O_{3-x/2-\delta}$ $(0 \leq x \leq 0.15)$ were chosen to study the improvement of n-type conductivity in perovskite oxides by enhancing bulk oxide ion mobility.[101] The study suggested that both oxygen deficiency (δ) and conductivity (σ) of the reduced $La_{0.4}Sr_{0.4}Ga_xTi_{1-x}O_{3-x/2-\delta}$ were increased significantly with Ga doping. The oxygen deficiency was increased from 0.035 to 0.060 when Ga stoichiometry was enhanced from $x = 0$ to $x = 0.15$ after reduction. The corresponding conductivity values were also increased with doping and showed a maximum conductivity of 50 S cm^{-1} for $x = 0.05$. They also found that the Ga doping could promote a fast reduction of the samples and significantly increase the stability of the reduced phase in oxidizing conditions at high temperatures.

$La_{1-x}Sr_xSc_{1-y}Ti_yO_{3-d}$ (LSST) was synthesized through a glycine nitrate process by Hatchwell *et al.*[102] A-site deficiency led to an increased ionic conductivity over LSST. The highest total conductivity achieved for $(La_{0.8}Sr_{0.2})_{0.99}Sc_{0.9}Ti_{0.1}O_{3-d}$ in air with ~1% H_2O at 800 °C was 23 mS cm^{-1}, in which 6 mS cm^{-1} was ionic. Li *et al.*[103] found that the Sc-doping in LST increased

the oxygen vacancy concentration and decreased the oxygen migration energy. The ionic conductivity of $La_{0.3}Sr_{0.7}Sc_{0.1}Ti_{0.9}O_{3-\delta}$ was 1×10^{-2} S cm^{-1} at 800 °C at the oxygen partial pressure of 10^{-19} atm. This value increased about 230% compared with pure $La_{0.3}Sr_{0.7}TiO_{3-\delta}$.

Gorte *et al.*[104] thought that the morphologies design and control synthesis of anode were particularly crucial because a larger triple phase boundary (TPB) and the thermal compatibility were required to obtain high fuel cell performance. Based on this viewpoint, Chang *et al.*[105] reported a novel core–shell anode material, which was prepared with Nb-doped LST perovskite core of $(La_{0.3}Sr_{0.7})(Ti_{1-x}Nb_x)O_3$ (LSTNx) and the shell of multiple elements doped ceria $(La_{0.75}Sr_{0.2}Ba_{0.05})_{0.175}$-$Ce_{0.825}O_{1.891}$ (LSBC) by a citric acid-based combustion coating process. The obtained LSTNs powders morphologies were shown in Fig. 6a and c. The elemental analysis on the core–shell SLTN0.1–12 mol% LSBC powders was shown in Fig. 6b. The shell LSBC nanoparticles adhered on the larger calcined SLTN0.1 core particles were distinguished, as shown in Fig. 6c. It indicated the element of Ce existed on the nanoparticles of the shell (Fig. 6e), which further proved the core–shell formation. The Sr and Ti distributed over core–shell main body (Fig. 6d and f). The Sr and Ti mapping images indicated the core SLTN also existed below the nanoparticles except the large core as seen at the center of Fig. 6c. The power density increased three times by using the core–shell structural anode than that without using the core–shell anode in a half-cell test. This can be attributed to the increased the effective TPB sites and the reduced the interface thermal expansion and lattice matching, as well as extended the ionic conduction path from the LSBC electrolyte to the core–shell anode. The authors thought that the benefits of core–shell structure include simple anode material and structure preparation for the anode without the tedious mixing or impregnation of secondary functional particles. It was also suggested that the core–shell structured anode could be applied in the design of other anode materials.

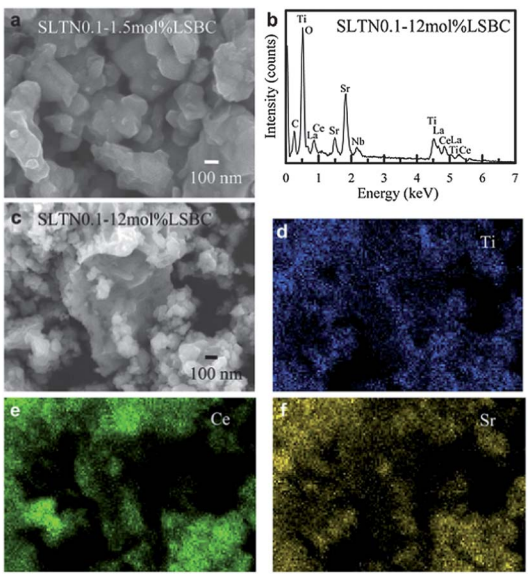

Fig. 6 FESEM images and EDS elemental analysis of the prepared core–shell anode powders, (a) FESEM image of LSTN0.1–1.5 mol% LSBC, (b) EDS pattern of LSTN0.1–12 mol% LSBC, (c) FESEM image of LSTN0.1–12 mol% LSBC, and the EDS elemental mappings on the LSTN0.1–12 mol% LSBC, (d) Ti, (e) Ce as well as (f) Sr. Reprinted from ref. 105, Copyright (2012), with permission from International Association for Hydrogen Energy.

3.3 LST-based composite anode materials

Combining LST with other conductor or active catalyst to form a composite anode is an effective way to improve the conductivity and electrocatalytic performance. In this part of the review, the developments of the LST-based composite anode materials are summarized.

3.3.1 Direct addition to LST. It is well known that the LST materials showed poor electro-catalytic performance. As a good catalyst, CeO_2 may enhance the overall electrochemical performance. Composite anode materials including LST and CeO_2-based additives such as $La_{0.20}Sr_{0.25}Ca_{0.45}TiO_3$ + CeO_2,[79] $La_{0.20}Sr_{0.25}Ca_{0.45}TiO_3$ + CeO_2 + Ni,[79] $La_{0.4}Sr_{0.6}Ti_{0.8}Mn_{0.2}O_{3\pm\delta}$ + CeO_2 + Pd,[86] $La_{0.3}Sr_{0.7}TiO_3$ + CeO_2 + Pd[107,108,110] have been reported in the above work. $La_{0.4}Sr_{0.6}TiO_3$ (LST) was ball milled with different weight ratios of CeO_2.[106] Increasing CeO_2 content in LST matrix decreased the cell polarization resistance and increased the maximum power density. The cell with LST–50 wt% CeO_2 anode created maximum power densities of about 172.3, 139.6 mW cm^{-2} in humidified H_2 and CH_4 at 900 °C, respectively. The higher fuel cell performances were attributed to the additional amount of CeO_2, which extended the anode TPBs.

Ahn *et al.*[62] have studied YSZ and $La_{0.3}Sr_{0.7}TiO_3$ (LST) composite support layer for SOFCs. Excellent performance of the SOFCs was obtained using an anode having a functional layer made from Pd-doped CeO_2 in YSZ and a current collector from LST.[107] The maximum power densities were 208 mW cm^{-2} at 973 K and 539 mW cm^{-2} at 1073 K using humidified CH_4 as fuel. At the same time, the anode showed no evidence for carbon formation during an overnight exposure to CH_4. They also found that the functional layer could be prepared by impregnation of 1 wt% Pd and 10 wt% CeO_2 into porous LST and YSZ.[108] This strategy allowed much greater flexibility in electrode design to include different layers. Furthermore, the performance of the LST + Pd-doped CeO_2 in YSZ was considered to be only modest. The conductivities of composites with 35 vol% LST were only 0.1 S cm^{-1} at 1173 K in humidified H_2, more than 200 lower than the value reported for bulk LST.[109] LST was added to porous YSZ by infiltration method to form LST–YSZ composite anode materials.[110] The conductivity of this composite depended strongly on the pretreatment conditions but was greater than 0.4 S cm^{-1} after being heated to 1173 K in humidified H_2. With the addition of 0.5 wt% Pd and 5 wt% CeO_2, the maximum power density of LST–YSZ composite anode materials increased from less than 20 to 780 mW cm^{-2} for operating in humidified H_2 at 1073 K. Hill *et al.*[111] investigated the electrochemical conversion pathway of CH_4 on Ni/YSZ and $La_{0.3}Sr_{0.7}TiO_3$ bi-layer anode materials in details. They found that the pathway include the CH_4 decomposition and subsequent oxidation C and H_2, which strongly depended on the anode polarization.

Based on the LST–CeO_2 composite anode materials, different doped CeO_2 including GDC (Gd-doped CeO_2), YDC (Y-doped CeO_2), SDC (Sm-doped CeO_2), LDC (La-doped CeO_2) *etc.* were further explored as the additive to improve the performance of LST-based anode materials.

The addition of GDC to LST has been proved to be an efficient way to improve the performance of the cell in the above mentioned work.[83,94,97] Dense and porous A-site deficient $La_{0.2}Sr_{0.7}TiO_3$ were prepared by Savaniu *et al.*[112] Two types of fuel cells, electrolyte supported and anode supported, were produced using YSZ as the electrolyte, porous LST impregnated with $Ce_{0.8}Gd_{0.2}O_2$ and Cu as the anode, and $La_{0.6}Sr_{0.4}CoO_3$ as the cathode. Maximum power densities of 0.22 and 0.5 W cm^{-2} at 750 °C were achieved using dense and porous $La_{0.2}Sr_{0.7}TiO_3$ in humidified H_2, respectively. In another work, $La_{0.2}Sr_{0.8}TiO_3$ powers were mixed with $Ce_{0.8}Gd_{0.2}O_{2-\delta}$ (GDC) powders in 50 : 50 weight ratio to form LST–GDC composite in which Ni was impregnated afterwards.[113] GDC could provide the ionic conduction path whereas the small amount of Ni would enhance the catalytic activity. The polarization resistance (R_p) of LST–GDC anode was greatly reduced relative to that of pure LST anode. When Ni was impregnated into LST–GDC composite, the R_p value was further reduced to 1 Ω cm^2 at 800 °C in humidified H_2 (Fig. 7), which was ~10% of that for pure LST anode. The maximum power density of the single cell with LST–GDC + Ni anode was about 275 mW cm^{-2} at 800 °C, much larger than 60 mW cm^{-2} for the cell with LST–GDC anode. A similar study was conducted in ref. 114 in which $La_{0.2}Sr_{0.8}TiO_3$–GDC–Ni anodes of various composition ratios were prepared as the anode. With LSGM as the electrolyte and $La_{0.6}Sc_{0.4}Co_{0.2}Fe_{0.8}O_3$ (LSCF) as the cathode material at 800 °C in humidified H_2, the performance of single cell was about 300 mW cm^{-2}, increasing drastically from 67 mW cm^{-2} for the cell without Ni impregnation. It was suggested that in order to further reduce the polarization resistance, the optimization of anode microstructure and the content and distribution of Ni particles might be helpful. A-site deficient LST backbone impregnated with GDC and Ni[115] or Cu[116] was also investigated by Savaniu *et al.* A-site deficient $La_{0.2}Sr_{0.7}TiO_3$ was impregnated using solutions with 20 mol% GDC and a metal Cu. YSZ and $La_{0.6}Sr_{0.4}CoO_3$ (LSC) thin layer were used as the electrolyte and the cathode material, respectively. Fuel cells tests demonstrated that remarkable power densities about 0.5 W cm^{-2} at 750 °C could be achieved using pure, humidified H_2 as fuel.

$Y_{0.2}Ce_{0.8}O_{2-\delta}$ (YDC) was also explored as the additive to LST-based composite because of its high ionic conductivity and catalytic performance. It was found that $La_{0.4}Sr_{0.6}TiO_{3\pm\delta}$ (LST) and YDC composite was a stable, high performance material for use as anode in SOFCs fed by 0.5% H_2S-containing syngas, whereas pure CeO_2 was not chemically stable using the same fuel.[117] Moreover, both LST and YDC were synthesized using citrate–nitrate gel combustion method.[118] The obtained LST and YDC powders were ball-milled and calcined to obtain the LST–YDC composite anode. The maximum power densities at 850 °C were 169, 102 and 39 mW cm^{-2} when the cell was fueled with syngas having 0.5% H_2S, pure syngas and 0.5% H_2S balanced with Ar, respectively. Gas chromatographic and mass spectrometric analyses revealed that the presence of H_2S improved the rate of fuel electrochemical oxidation while H_2S itself was not converted and its oxidation was not the source of the enhanced performance. The presence of H_2S in different feeds was evidenced to have negligible influence over the fuel cell stability.

Pillai *et al.*[119] studied the SOFCs with $La_{0.2}Sr_{0.8}TiO_3$ anode-side supports, along with NiO–$Ce_{0.8}Sm_{0.2}O_2$ (SDC) (1 : 1 by weight) adhesion layer, NiO–YSZ (1 : 1 by weight) anode active layer, YSZ electrolyte, and LSM–YSZ cathode. The colloidal solutions of NiO–SDC, NiO–YSZ, and YSZ were sequentially dropped and coated onto the LST pellets. The obtained LST-supported SOFCs showed improved stability against coking in natural gas, compared with conventional Ni–YSZ anode-supported SOFCs. There was no long-term degradation in H_2 fuel with 50–100 ppm H_2S, and no degradation during redox cycling. However, the maximum power density was decreased from 850 mW cm^{-2} to about 700 W cm^{-2} when the fuel was changed from dry H_2 to dry H_2 containing 100 ppm H_2S, which further indicated the poor sulfur tolerance of Ni-based catalyst.

Besides the CeO_2-based oxide, the addition of Bi_2O_3 into LST was also reported to be able to significantly reduce the fuel cell's polarization, refine the grains, increase the triple phase boundary, and then to improve the electrochemical performance.[120]

3.3.2 Exsoluted nanoparticles from doped LST. Certain doping elements in LST were not stable in reducing environment at elevated temperature. They tended to exsolute from the LST matrix and form nano-scale electrocatalytic active particles which promoted the anode performance considerably. As mentioned in the above doped LST-based materials, different nanoparticles such as electrocatalytic active nano Ce-rich phase[75] (see Fig. 3), Ni,[92,99] Co[96] and Fe[99] nanoparticles were exsoluted to the LST surfaces. Ru nanoparticles exsoluted from $La_{0.8}Sr_{0.2}Cr_{0.82}Ru_{0.18}O_{3-\delta}$,[121] Ni nanoparticles from $La_{0.8}Sr_{0.2}Cr_{1-y}Ni_yO_{3-\delta}$[122] and Ni, Cu, Co nanoparticles from $Ce_{1-x}M_xVO_{4-0.5x}$ (M = Ni, Co, Cu)[123] were also observed. Thereby, the resulting nanoparticles extended the length of TPB

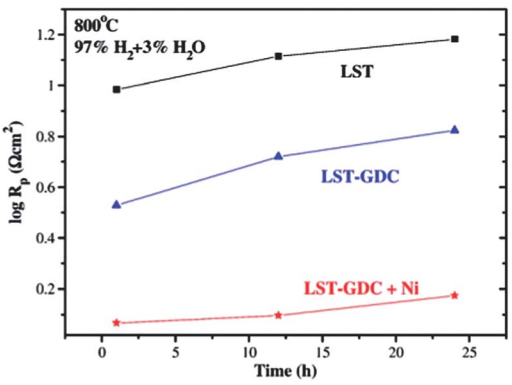

Fig. 7 The polarization resistance values of symmetrical LSGM electrolyte-supported cell with LST, LST–GDC and Ni-impregnated LST–GDC anodes as a function of time. All data were extracted from the impedance spectra obtained under open circuit conditions at 800 °C. All values increased with time. Reprinted from ref. 113, Copyright (2009), with permission from Elsevier.

and enhanced the fuel cell performance. Recently, Neagu *et al.* investigated the metallic, oxides or mixtures nanoparticles *in situ* growth on the surface of stoichiometry or non-stoichiometry LST.[124]

Although the nanostructured electrocatalytic active composition exsoluted from the doped LST matrix is a potential way to form high performance LST composite anode. The effective control of the exsoluted particle quantity and the prevention of their aggregation at high temperature are crucial and remain to be solved in future research. In addition, the LST-based composite anode materials including Ni nanoparticles could not be used directly for the hydrocarbon fuel because of their poor carbon resistance character.

3.4 LST synthesis methods

Overview of all the LST materials covered in this review suggests that conventional solid state method[53–60,62–67,71,76,78–80,85,90–96,100,101,108,115,116,119,120] was still the main route to prepare LST materials due to its simplicity and relatively low processing cost. However, the solid state method needs a long period of time to facilitate the diffusion at high temperature (usually >1200 °C). The obtained products were often coarse and agglomerated, exhibiting limited purity and homogeneity. Therefore, the new approaches for the development of nano-structured electrodes are needed and some soft ways have drawn increasing attentions in recent years.[125] The other different routes to synthesize LST-based materials include Pechini route,[61,75,82] impregnation or infiltration method,[77,86,107,110] combustion synthesis,[83,88] citric acid–nitrate process,[68,84,98,99,105,118] glycine–nitrate and citrate synthesis routes,[52,87,102] spray pyrolysis method,[72] and nanoparticle-based spray pyrolysis[70,74] to synthesize LST-based materials. The LST powders obtained through the above soft methods have small particle size and narrow size distribution or porous structure which would enlarge the TPBs and then improve the performance. Recently, Birol *et al.*[126] reviewed the cellulose-assisted glycine nitrate process of preparing ceramic nanoparticles. Some other soft methods such as co-precipitation method,[127] sol–gel route[128] and rheological phase reaction[129,130] were the potential techniques to synthesize LST-based anode materials.

For the synthesis of LST composite anode materials, the common way was to mix pure LST with other materials automatically.[62,74,106,108,113,114,120,137] Impregnation or infiltration technology[107,110,112,116] was another commonly used and effective way to add the active components to the LST materials. Combination of the combustion method and automatical mix,[118] colloidal deposition technique[119] were also applied to blend LST and other materials. Exsolution method was a compellent way to obtain LST-based anode materials[76,92,96,99,121–123] and would be further explored in the future work.

3.5 Conductivity and performance of LST-based anode materials

Table 1 summaries the conductivities of selected LST-based anode materials. We can see that the pure $SrTiO_3$ has a low ionic conductivity. The co-doped La and other metal ions in A-site and B-site doping can obviously improve the conductivity. The type of doping element and the doping quantity should be experimentally optimized in the future work.

Table 1 Conductivity of selected LST-based anode materials

Anode composition	Electronic conductivity (S cm^{-1})	Ionic conductivity (S cm^{-1})	Tem. (°C)	Fuel	Ref.
$La_{0.6}Sr_{0.1}TiO_{3-\delta}$	7	—	930	5% H_2/Ar	54
$La_2Sr_4Ti_6O_{19-\delta}$	40	—	950	5% H_2/Ar	58
$La_{0.4}Sr_{0.4}TiO_3$	~100	—	900	5% H_2/Ar	60
$La_{0.3}Sr_{0.7}TiO_{3-\alpha}$	~100	—	1000	9% H_2/N_2	63
$La_{0.1}Sr_{0.9}TiO_3$	12	—	1000	30% H_2/N_2	68
$(La_{0.3}Sr_{0.7})_{0.93}TiO_{3-\delta}$	145	1.0×10^{-2}	800	5% H_2/Ar	69
$La_{0.2}Sr_{0.7}TiO_3$	0.3	—	800	5% H_2/Ar	72
$La_{0.2}Sr_{0.7}TiO_3$	30–40	—	1000	5% H_2/Ar	
$La_{0.2}Sr_{0.7}TiO_3$	~100	—	1200	5% H_2/Ar	
$La_{0.2}Sr_{0.7}TiO_3$	600	—	600	5% H_2/N_2	70
$La_{0.2}Sr_{0.25}Ca_{0.45}TiO_3$	27.53	—	900	5% H_2/Ar	80
$La_{0.3}Sr_{0.55}Ti_{0.8}Cr_{0.2}O_{3-\delta}$	1.96×10^{-3}	—	800	Static air	84
$La_{0.3}Sr_{0.7}Ti_{0.8}Cr_{0.2}O_{3-\delta}$	53	—	800	5% H_2/Ar	85
$La_{0.33}Sr_{0.67}Ti_{0.92}Al_{0.08}O_{3+\delta}$	1.5	—	900	5% H_2/Ar	91
$La_{0.33}Sr_{0.67}Ti_{0.92}Sc_{0.08}O_{3+\delta}$	5.5	—	900	5% H_2/Ar	
$SrTiO_3$	0.03	—	700	5% H_2/Ar	95
$La_{0.3}Sr_{0.7}TiO_{3-\delta}$	247	1×10^{-3}	700	5% H_2/Ar	
$La_{0.3}Sr_{0.7}Co_{0.07}Ti_{0.93}O_{3-\delta}$	63	6×10^{-3}	700	5% H_2/Ar	
$La_{0.5}Sr_{0.5}Ti_{0.75}Ni_{0.25}O_{3-\delta}$	2.2×10^{-3}	—	800	Air	99
$La_{0.5}Sr_{0.5}Ti_{0.75}Ni_{0.25}O_{3-\delta}$	4.9×10^{-4}	—	800	2% H_2/Ar	
$La_{0.5}Sr_{0.5}Ti_{0.75}Ni_{0.25}O_{3-\delta}$	2.3	—	800	2% H_2/Ar	
$La_{0.4}Sr_{0.4}Ga_{0.05}Ti_{0.95}O_{2.95/2-\delta}$	~50	—	880	5% H_2/Ar	101
$(La_{0.8}Sr_{0.2})_{0.99}Sc_{0.9}Ti_{0.1}O_{3-d}$	6×10^{-3}	—	800	1% H_2O/air	102
$La_{0.3}Sr_{0.7}Sc_{0.1}Ti_{0.9}O_{3-\delta}$	49	1×10^{-2}	800	5% H_2/Ar	103
$La_{0.3}Sr_{0.7}TiO_3$	>0.4	—	900	3% H_2O/H_2	110

Table 2 lists the fuel cell performances of selected LST-based anode materials. It can be seen that the pure LST materials have a poor electrocatalytic performance for H_2 oxidation. The common methods to improve the performance include: (1) exploring new methods to synthesize LST-based anode materials with a nanostructure; (2) mixing, impregnation or infiltration of high ionic conductor (CeO_2-based materials, Bi_2O_3, *etc.*) and high catalytic materials (Pd, Cu, Ni, *etc.*) into porous LST; (3) exsolution method is a potential technology to form LST-based composite anode materials.

4. H_2S-induced enhancement for electrochemical reaction on LST-based anode materials

H_2S is a common impurity in many industrial feedstocks such as coal derived syngas and raw natural gas. Although H_2S may serve as an increasingly significant source for sulfur production, it is a major industrial pollutant that is toxic and corrosive. Direct electrochemical conversion of H_2S in SOFCs would offer both economical and environmental benefits.[131–135] It is known that even trace amount of H_2S could lead to severe performance degradation of the fuel cells when using Ni-based anode materials.[24–26] Therefore, a series of LST-based anode materials have been developed in our lab, which showed not only a high H_2S poisoning resistance and high chemical stability but also a H_2S-induced enhancement effect for electrochemical reaction when using a fuel containing H_2S.

The sulfur tolerance of $La_{1-x}Sr_xBO_3$/YSZ anodes (B = Mn, Cr, and Ti) was examined at 1273 K in a H_2/H_2O fuel using YSZ electrolyte, LSM cathode.[136] The study indicated that the $La_{0.4}Sr_{0.6}TiO_3$ anode showed no degradation in the presence of up to 5000 ppm of H_2S in H_2. It was found that the performance of the fuel cell improved significantly in the presence of 5000 ppm of H_2S especially at the higher current densities. But the reason for this improvement was not clear in this work. The sulfur tolerance of the perovskite-based anodes decreased in the order $La_{0.4}Sr_{0.6}TiO_3$ (LST) > $La_{1-x}Sr_xCrO_3$ (LSC) > $La_{1-x}Sr_xMn_yCr_{1-y}O_3$ (LSCM).

Table 3 compares the fuel cell performances of LST-based anode materials when the fuel contained trace amount of H_2S. It is clearly shown that the performance was dramatically improved when H_2S was present in the fuels such as

Table 2 Fuel cell performance of selected LST-based anode materials

Anode composition	Electrolyte (thickness)/cathode	Tem. (°C)	Fuel	MPD[a] (mW cm^{-2})	Ref.
$La_{0.4}Sr_{0.6}TiO_3$	YSZ (160 μm)/LSM	1000	Humidified H_2	260	52
$La_2Sr_4Ti_6O_{19-\delta}$	YSZ (2 mm)/LSM	900	Humidified H_2	76	59
$La_{0.3}Sr_{0.7}TiO_3$ + CeO_2 + Cu	YSZ (60 μm)/LSM	700	H_2	200	62
$La_{0.2}Sr_{0.8}TiO_3$	YSZ (280 μm)/Pt	900	5% H_2 + 95% Ar	12	71
$La_{0.4}Sr_{0.45}Ba_{0.15}TiO_3$	YSZ (300 μm)/LSM	850	H_2	~39	76
$La_{0.4}Sr_{0.5}Ba_{0.1}TiO_3$	YSZ (300 μm)/LSM	850	H_2	20	77
$La_{0.20}Sr_{0.25}Ca_{0.45}TiO$ + CeO_2 + Ni	ScSZ (310 μm)/LSM	900	Humidified H_2	~300	79
$La_{0.3}Sr_{0.7}TiO_{3-\delta}$	YSZ (400 μm)/LSM	900	Humidified H_2	~31	85
$La_{0.3}Sr_{0.7}Ti_{0.8}Cr_{0.2}O_{3-\delta}$				44	
$La_{0.4}Sr_{0.6}Ti_{0.8}Mn_{0.2}O_{3\pm\delta}$	YSZ (50 μm)/LSM	800	Humidified H_2	30	86
$La_{0.4}Sr_{0.6}Ti_{0.8}Mn_{0.2}O_{3\pm\delta}$ + Pd				~70	
$La_{0.4}Sr_{0.6}Ti_{0.8}Mn_{0.2}O_{3\pm\delta}$ + CeO_2				100	
$La_{0.4}Sr_{0.6}Ti_{0.8}Mn_{0.2}O_{3\pm\delta}$ + Pd + CeO_2				150	
$La_{0.6}Sr_{0.4}Ti_{0.2}Mn_{0.8}O_{3-\delta}$	GDC (500 μm)/$Ba_{0.6}Sr_{0.4}Co_{0.5}Fe_{0.5}O_{3-\delta}$	800	Humidified H_2	290	88
$La_{0.2}Sr_{0.8}Ti_{0.98}Co_{0.02}O_3$ + GDC + Ni	LSGM (500 μm)/$Ba_{0.5}Sr_{0.5}Co_{0.8}Fe_{0.2}O_{3-\delta}$	800	Humidified H_2	250	94
$La_{0.3}Sr_{0.7}TiO_{3-\delta}$	YSZ (300 μm)/LSM	900	Humidified H_2	90	96
$La_{0.3}Sr_{0.7}Ti_{0.93}Co_{0.07}O_{3-\delta}$				230	
$La_{0.2}Sr_{0.8}Ti_{0.98}Co_{0.02}O_3$ + GDC + Ni	LSGM (250 μm)/$La_{0.6}Sr_{0.4}Co_{0.2}Fe_{0.8}O_{3-\delta}$	800	Humidified H_2	638	97
$La_4Sr_8Ti_{11}Mn_{0.5}Ga_{0.5}O_{37.5}$	YSZ (2 mm)/LSM	950	Humidified H_2	500	100
$La_{0.4}Sr_{0.6}TiO_3$ + CeO_2	YSZ (300 μm)/ScSz + LSM	900	Humidified H_2	172	106
$La_{0.3}Sr_{0.7}TiO_3$	YSZ (60 μm)/LSF	800	Humidified H_2	20	110
$La_{0.3}Sr_{0.7}TiO_3$ + CeO_2 + Pd				780	
$La_{0.3}Sr_{0.7}TiO_3$ + Ni/YSZ	YSZ (300 μm)/Pt	750	Humidified H_2	102	111
Dense $La_{0.2}Sr_{0.7}TiO_3$ + GDC + Cu	YSZ (150 μm)/$La_{0.6}Sr_{0.4}CoO_3$ (LSC)	750	Humidified H_2	220	112
Porous $La_{0.2}Sr_{0.7}TiO_3$GDC + Cu				500	
$La_{0.2}Sr_{0.8}TiO_3$ + GDC	LSGM (500 μm)/$Ba_{0.5}Sr_{0.5}Co_{0.8}Fe_{0.2}O_{3-\delta}$	800	Humidified H_2	60	113
$La_{0.2}Sr_{0.8}TiO_3$ + GDC + Ni	(BSCF)			275	
$La_{0.2}Sr_{0.8}TiO_3$ + GDC	LSGM (150 μm)/$La_{0.6}Sc_{0.4}Co_{0.2}Fe_{0.8}O_3$	800	Humidified H_2	67	114
$La_{0.2}Sr_{0.8}TiO_3$ + GDC + Ni	(LSCF)			300	
$La_{0.44}Sr_{0.56}TiO_3$ + GDC + Ni	YSZ (32 μm)/LSC64	850	Humidified H_2	185	115
$La_{0.2}Sr_{0.7}TiO_3$ + GDC + Cu	YSZ (50–75 μm)/$La_{0.6}Sr_{0.4}CoO_3$	750	Humidified H_2	500	116
$La_{0.4}Sr_{0.6}TiO_{3\pm\delta}$ + YDC	YSZ (300 μm)/LSM	850	40% H_2 + 60% CO	102	118
$La_{0.2}S_{r0.8}TiO_3$ + NiO–SDC + NiO–YSZ	YSZ/LSM	800	Dry H_2	850	119
$La_{0.4}Sr_{0.6}TiO_3$	YSZ (500 μm)/LSM	1000	Humidified H_2	175	136

[a] MPD = maximal power density.

Table 3 Fuel cell performance of LST-based anode materials using fuel containing H_2S

Anode composition	Electrolyte/cathode	Tem. (°C)	Fuel	MPD[a] (mW cm^{-2})	Ref.
$La_{0.4}Sr_{0.45}Ba_{0.15}TiO_3$	YSZ (300 μm)/LSM	850	H_2	~39	76
			H_2 + 0.5% H_2S	~50	
			CH_4	~1.5	
			CH_4 + 0.5% H_2S	~7.5	
$La_{0.4}Sr_{0.5}Ba_{0.1}TiO_3$	YSZ (300 μm)/LSM	850	H_2	20	77
			H_2 + 0.5% H_2S	137	
			CH_4	24	
			CH_4 + 0.5% H_2S	75	
$La_{0.3}Sr_{0.55}Ti_{1-x}Cr_xO_{3-\delta}$	YSZ (300 μm)/Pt	900	CH_4	~2	83
			CH_4 + 0.5% H_2S	~140	
$La_{0.3}Sr_{0.7}Ti_{0.93}Co_{0.07}O_{3-\delta}$	YSZ (300 μm)/LSM	900	H_2	230	96
			H_2 + 0.5% H_2S	300	
$La_{0.4}Sr_{0.6}TiO_{3\pm\delta}$ + YDC	YSZ (300 μm)/LSM	850	40% H_2 + 60% CO	102	118
			40% H_2 + 60% CO + 0.5% H_2S	169	
$La_{0.2}S_{r0.8}TiO_3$ + NiO–SDC + NiO–YSZ	YSZ/LSM	800	Dry H_2	850	119
			Dry H_2 + 100 ppm H_2S	700	
$La_{0.4}Sr_{0.6}TiO_3$	YSZ (500 μm)/LSM	1000	Humidified H_2	175	136
			Humidified H_2 + 0.5% H_2S	~210	
$La_{0.4}Sr_{0.6}TiO_{3-\delta}$	YSZ/Pt	850	CH_4	~2	137
			CH_4 + 5% H_2S	320	
			CH_4 + 20% H_2S	450	

[a] MPD = maximal power density.

CH_4,[76,77,83,137] H_2,[76,77,136] syngas (H_2 + CO)[117,118]. This can also be observed clearly in Fig. 8. In ref. 119, the performance was decreased when using the dry H_2 containing 100 ppm H_2S, which could be attributed to the poisoning of Ni-based active catalyst in LST-based composite anode.

A series of experiments were designed to systematically investigate the electrochemical performance and compositions of anode gases to explore the mechanism of the significant performance enhancement with H_2S presence in either CH_4 or H_2 fuel. $La_{0.4}Sr_{0.6}TiO_{3-\delta}$ was mixed with commercial YSZ power with a 50/50 weight ratio to form the anode materials.[137] Platinum paste was used as the cathode and the current collector. Electrolyte was the commercial YSZ dicks. The power density improved dramatically from 2 mW cm^{-2} with pure CH_4 as fuel to more than 450 mW cm^{-2} for CH_4 containing 20% H_2S (Fig. 8). From thermodynamic calculations and mass spectroscopic data obtained at different potential stages during a regular potentiodynamic run, it was concluded that H_2S was not the only fuel converted, and its interaction with CH_4 was the key factor for the enhancement of performance. The anode effluent gas mixture included H_2S, SO_2, H_2 and CS_2, which was consistent with thermodynamic predictions. The conclusion was that H_2S had a synergistic effect on CH_4 oxidation, *i.e.*, CH_4 and H_2S must not be considered as two separate fuels. H_2S actually ran as a powerful promoter for fuel electro-oxidation. At low current density, there was a rapid conversion of surface species, whereas at high current density there was a mass transfer blocking effect from build-up of the surface intermediates. The predominant form of sulfur in the gas phase was H_2S previously presented. There was at least 3% H_2 in the mixture. CH_4 conversion proceeded *via* rapid formation of syngas, and the reaction path probably included CS_2 and other sulfur species. The selectivity of the obtained products could be controlled by adjusting the applied voltage. In order to further explore the mechanism of the H_2S enhancement effect in details, *in situ* technologies such as *in situ* Raman,[138] *in situ* XPS[139] *etc.* were recommended to be applied in the field in the future work.

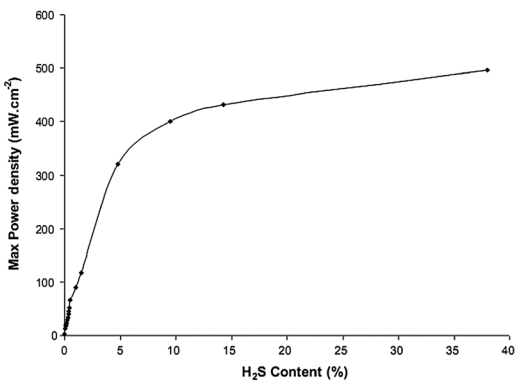

Fig. 8 Maximal power density (after compensation) as a function of H_2S concentration in CH_4 (after flow corrections) at 850 °C. Fuels were fed at 50 mL min^{-1}. Reprinted from ref. 137, Copyright (2011), with permission from Elsevier.

5. Conclusions

The recent progress in the field of LST-based anode materials in SOFCs are summarized. Although pure LST had very limited activity for oxidation of H_2S-free fuels, it exhibited superior balance between high chemical stability in sulfur/carbon environment and adequate electrical conductivity compared to other anode candidates. Thus it could be used as an anode

matrix material and its properties could be further tailored depending on the fuel selected. Doping and composting of LST are the most effective ways to increase the ionic conductivity and the electrocatalytical activity of LST-based anode.

Future work on the LST-based anode materials in SOFCs can focus on the following aspects: (1) Exploring new methods to synthesize LST materials, doping LST with appropriate elements in different site, impregnating, mixing or coating nano-structured ionic conductor or exsoluted electrocatalytical active nanoparticles to LST anode. (2) Combining LST-based materials with other catalytic active material to form LST-based composite anode materials using impregnation, infiltration technique or some other new methods. The added secondary phases should sustain sufficient thermal stability at elevated temperature. (3) Exploring the fuel conversion mechanism of LST-based anode especially the H_2S-induced enhancement effect for electrochemical reaction using *in situ* experimental technologies.

Acknowledgements

This research was supported through funding to the Solid Oxide Fuel Cell Canada Strategic Research Network and Strategic Grant from the Natural Science and Engineering Research Council (NSERC).

Notes and references

1 K. Onda, T. Iwanari, N. Miyauchi, K. Ito, T. Ohba, Y. Sakaki and S. Nagata, *J. Electrochem. Soc.*, 2003, **150**, A1569.
2 A. J. Jacobson, *Chem. Mater.*, 2010, **22**, 660.
3 C. Sun, R. Hui and F. Roller, *J. Solid State Electrochem.*, 2010, **14**, 1125.
4 Z. Jiang, C. Xia and F. Chen, *Electrochim. Acta*, 2010, **55**, 3595.
5 E. D. Wachsman and K. T. Lee, *Science*, 2011, **334**, 935.
6 E. Fabbri, D. Pergolesi and E. Traversa, *Chem. Soc. Rev.*, 2010, **39**, 4355.
7 E. Fabbri, L. Bi, D. Pergolesi and E. Traversa, *Adv. Mater.*, 2012, **24**, 195.
8 M. Ni, *Int. J. Hydrogen Energy*, 2013, **38**, 2846.
9 L. Wu and X. Liu, *J. Mater. Sci. Technol.*, 2010, **26**, 293.
10 N. Shaigan, W. Qu, D. G. Ivey and W. Chen, *J. Power Sources*, 2010, **195**, 1529.
11 M. K. Mahapatra and K. Lu, *J. Power Sources*, 2010, **195**, 7129.
12 D. Coillot, F. O. Méar, H. Nonnet and L. Montagne, *Int. J. Hydrogen Energy*, 2012, **37**, 9351.
13 A. Sarikaya, V. Petrovsky and F. Dogan, *J. Electrochem. Soc.*, 2012, **159**, F665.
14 N. Yan, X. Z. Fu, J. L. Luo, K. T. Chuang and A. R. Sanger, *J. Power Sources*, 2012, **198**, 164.
15 K. Wang, D. Hissel, M. C. Péra, N. Steiner, D. Marra, M. Sorrentino, C. Pianese, M. Monteverde, P. Cardone and J. Saarinen, *Int. J. Hydrogen Energy*, 2011, **36**, 7212.
16 S. A. Hajimolana, M. A. Hussain, W. M. A. W. Daud, M. Soroush and A. Shamiri, *Renewable Sustainable Energy Rev.*, 2011, **15**, 1893.
17 A. Choudhury, H. Chandra and A. Arora, *Renewable Sustainable Energy Rev.*, 2013, **20**, 430.
18 L. Barelli, E. Barluzzi and G. Bidini, *Int. J. Hydrogen Energy*, 2013, **38**, 5060.
19 A. Atkinson, S. Barnett, R. J. Gorte, J. T. S. Irvine, A. J. Mcevoy, M. Mogensen, S. C. Singhal and J. Vohs, *Nat. Mater.*, 2004, **3**, 17–27.
20 P. I. Cowin, C. T. G. Petit, R. Lan, J. T. S. Irvine and S. Tao, *Adv. Energy Mater.*, 2011, **1**, 314.
21 X. M. Ge, S. H. Chan, Q. L. Liu and Q. Sun, *Adv. Energy Mater.*, 2012, **2**, 1156.
22 K. Gironaa, J. Laurencinb, J. Fouletierc and F. Lefebvre-Joud, *J. Power Sources*, 2012, **210**, 381.
23 K. T. Chuang, J. L. Luo and A. R. Sanger, *Chem. Ind. Chem. Eng. Q.*, 2008, **14**, 69.
24 Z. Cheng, J. H. Wang, Y. Choi, L. Yang, M. C. Lin and M. Liu, *Energy Environ. Sci.*, 2011, **4**, 4380.
25 M. Btesznowski, J. Jewulski and A. Zieleniak, *Cent. Eur. J. Chem.*, 2013, **11**, 960.
26 M. Ettler, H. Timmermann, J. Malzbender, A. Weber and N. H. Menzler, *J. Power Sources*, 2010, **195**, 5452.
27 G. Postole, K. Girona, J. Toyir, A. Kaddouri and P. Gélin, *Fuel Cells*, 2012, **12**, 275.
28 Y. Chen, Q. Liu, Z. Yang, F. Chen and M. Han, *RSC Adv.*, 2012, **2**, 12118.
29 L. Mlamar, B. Colldeforns, L. Yedra, S. Estradé, F. Peiró, A. Morata, T. Andreu and A. Tarancón, *J. Mater. Chem. A*, 2013, **1**, 4531.
30 A. Kelaidopoulou, A. Siddle, A. L. Dicks, A. Kaiser and J. T. S. Irvine, *Fuel Cells*, 2001, **1**, 219.
31 P. R. L. Keating, D. O. Scanlon and G. W. Watson, *J. Mater. Chem. C*, 2013, **1**, 1093.
32 C. Goulart and E. Djurado, *J. Eur. Ceram. Soc.*, 2013, **33**, 769.
33 J. W. Fergus, *Solid State Ionics*, 2006, **177**, 1529.
34 E. Lay, L. Dessemond and G. Gauthier, *J. Power Sources*, 2013, **221**, 149.
35 J. S. Park, J. Luo, L. Adijanto, J. M. Vohs and R. J. Gorte, *J. Power Sources*, 2013, **222**, 123.
36 Q. Ma, F. Tietz, A. Leonide and E. Ivers-Tiffée, *J. Power Sources*, 2011, **196**, 7308.
37 A. M. Hussain, J. V. T. Høgh, T. Jacobsen and N. Bonanos, *Int. J. Hydrogen Energy*, 2012, **37**, 4309.
38 S. W. Tao and J. T. S. Irvine, *J. Mater. Chem.*, 2002, **12**, 2356.
39 Y. H. Huang, R. I. Dass, Z. L. Xing and J. B. Goodenough, *Science*, 2006, **312**, 254.
40 H. Li, Y. Tian, Z. Wang, F. Qie and Y. Li, *RSC Adv.*, 2012, **2**, 3857.
41 X. Che, Y. Shen, H. Li and T. He, *J. Power Sources*, 2013, **222**, 288.
42 L. Troncoso, M. J. Martínez-Lope, J. A. Alonso and M. T. Fernández-Díaz, *J. Appl. Phys.*, 2013, **113**, 023511.
43 A. J. Weisentein, N. Childs, R. Amendola, D. Driscoll, S. W. Sofie, P. Gannon and R. Smith, *Mater. Chem. Phys.*, 2013, **139**, 706.
44 R. Martínez-Coronado, A. Aguadero, J. A. Alonso and M. T. Fernández-Díaz, *Solid State Sci.*, 2013, **18**, 64.
45 J. B. Goodenough, *Rep. Prog. Phys.*, 2004, **67**, 1915.

46 Y. Zheng, W. Zhou, R. Ran and Z. Shao, *Prog. Chem.*, 2008, **20**, 413.
47 I. Z. Rahman, M. A. Raza and M. A. Rahman, *Adv. Mater. Res.*, 2012, **445**, 497.
48 P. I. Cowin, C. T. G. Petit, R. Lan, C. J. Schaschke and S. Tao, *Solid State Ionics*, 2013, **236**, 48.
49 L. Adijanto, R. Küngas, J. Park, J. M. Vohs and R. J. Gorte, *Int. J. Hydrogen Energy*, 2011, **36**, 15722.
50 K. Singh, J. Nowotny and V. Thangadurai, *Chem. Soc. Rev.*, 2013, **42**, 1961.
51 K. Uematsu, O. Sakurai, N. Mizutani and M. Kato, *J. Mater. Sci.*, 1984, **19**, 3671.
52 O. A. Marina, N. L. Canfield and J. W. Stevenson, *Solid State Ionics*, 2002, **149**, 21.
53 R. Moos, T. Bischoff, W. Menesklou and K. H. Härdtl, *J. Mater. Sci.*, 1997, **32**, 4247.
54 P. R. Slater, D. P. Fagg and J. T. S. Irvine, *J. Mater. Chem.*, 1997, **7**, 2495.
55 D. Neagu and J. T. S. Irvine, *Chem. Mater.*, 2010, **22**, 5042.
56 A. Tesfai, C. Savaniu and J. T. S. Irvine, *ECS Trans.*, 2011, **35**, 557.
57 G. Tsekouras and J. T. S. Irvine, *J. Mater. Chem.*, 2011, **21**, 9367.
58 J. Canales-Vánzquez, W. Zhou and J. T. S. Irvine, *Ionics*, 2002, **8**, 252.
59 J. Canales-Vázquez, S. W. Tao and J. T. S. Irvine, *Solid State Ionics*, 2003, **159**, 159.
60 J. Canales-Vázquez, M. J. Smith, J. T. S. Irivine and W. Zhou, *Adv. Funct. Mater.*, 2005, **15**, 1000.
61 B. K. Park, J. W. Lee, S. B. Lee, T. H. Lim, S. J. Park, P. H. Song, W. B. Im and D. R. Shin, *Int. J. Hydrogen Energy*, 2012, **37**, 4319.
62 K. Ahn, S. Jung, J. M. Vohs and R. J. Gorte, *Ceram. Int.*, 2007, **33**, 1065.
63 S. Hashimoto, L. Kindermann, P. H. Larsen, F. W. Poulsen and M. Mogensen, *J. Electroceram.*, 2006, **16**, 103.
64 S. Hashimoto, F. W. Poulsen and M. Mogensen, *J. Alloys Compd.*, 2007, **439**, 232.
65 Y. Tsvetkova and V. Kozhukharov, *Mater. Des.*, 2009, **30**, 206.
66 Z. Wang, M. Mori and T. Itoh, *J. Electrochem. Soc.*, 2010, **157**, B1783.
67 M. Mori, Z. Wang, T. Itoh, S. Yabui, K. Murai and T. Moriga, *J. Fuel Cell Sci. Technol.*, 2011, **8**, 051014.
68 Z. Wang and M. Mori, *J. Fuel Cell Sci. Technol.*, 2011, **8**, 051018.
69 X. Li, H. Zhao, X. Zhou, N. Xu, Z. Xie and N. Chen, *Int. J. Hydrogen Energy*, 2010, **35**, 7913.
70 D. Burnat, A. Heel, L. Holzer, D. Kata, J. Lis and T. Graule, *J. Power Sources*, 2012, **201**, 26.
71 X. Huang, H. Zhao, W. Qiu, W. Wu and X. Li, *Energy Convers. Manage.*, 2007, **48**, 1678.
72 Q. Ma and F. Tietz, *Solid State Ionics*, 2012, **225**, 108.
73 S. Suthirakun, S. C. Ammal, G. Xiao, F. Chen, K. Huang, H. C. Loye and A. Heyden, *Solid State Ionics*, 2012, **228**, 37.
74 D. Burnat, A. Heel, L. Holzer, E. Otal, D. Kata and T. Graule, *Int. J. Hydrogen Energy*, 2012, **37**, 18326.
75 C. Périllat-Merceroz, G. Gauthier, P. Roussel, M. Huvé, P. Gélin and R. N. Vannier, *Chem. Mater.*, 2011, **23**, 1539.
76 A. Vincent, J. L. Luo, K. T. Chuang and A. R. Sanger, *J. Power Sources*, 2010, **195**, 769.
77 A. L. Vincent, A. R. Hanifi, J. L. Luo, K. T. Chuang, A. R. Sanger, T. H. Etsell and P. Sarkar, *J. Power Sources*, 2012, **215**, 301.
78 J. H. Li, X. Z. Fu, J. L. Luo, K. T. Chuang and A. R. Sanger, *J. Power Sources*, 2012, **213**, 69.
79 M. C. Verbraeken, B. Iwanschitz, A. Mai and J. T. S. Irvine, *J. Electrochem. Soc.*, 2012, **159**, F757.
80 A. D. Aljaberi and J. T. S. Irvine, *J. Mater. Chem. A*, 2013, **1**, 5868.
81 A. Yaqub, C. Savaniu, N. K. Janua and J. T. S. Irvine, *J. Mater. Chem. A*, 2013, DOI: 10.1039/c3ta12860a.
82 M. González-Cuencal, W. Zipprich, B. A. Boukamp, G. Pudmich and F. Tietz, *Fuel Cells*, 2001, **1**, 256.
83 N. Danilovic, A. Vincent, J. L. Luo, K. T. Chuang, R. Hui and A. R. Sanger, *Chem. Mater.*, 2010, **22**, 957.
84 F. Yi, H. Li, H. Chen, R. Zhao and X. Jiang, *Ceram. Int.*, 2013, **39**, 347.
85 Z. Du, H. Zhao, X. Zhou, Z. Xie and C. Zhang, *Int. J. Hydrogen Energy*, 2013, **38**, 1068.
86 J. H. Kim, D. Miller, H. Schlegl, D. McGrouther and J. T. S. Irvine, *Chem. Mater.*, 2011, **23**, 3841.
87 V. A. Kolotygin, E. V. Tsipis, A. I. Ivanov, Y. A. Fedotov, I. N. Burmistrov, D. A. Agarkov, V. V. Sinitsyn, S. I. Bredikhin and V. V. Kharton, *J. Solid State Electrochem.*, 2012, **16**, 2335.
88 M. K. Rath, B. G. Ahn, B. H. Choi, M. J. Ji and K. T. Lee, *Ceram. Int.*, 2013, **39**, 6343.
89 V. A. Kolotygin, E. V. Tsipis, M. F. Lü, Y. V. Pivak, S. N. Yarmolenko, S. I. Bredikhin and V. V. Kharton, *Solid State Ionics*, 2013, **251**, 28–33.
90 D. P. Fagg, V. V. Kharton, A. V. Kovalevsky, A. P. Viskup, E. N. Naumovich and J. R. Frade, *J. Eur. Ceram. Soc.*, 2001, **21**, 1831.
91 D. N. Miller and J. T. S. Irvine, *J. Power Sources*, 2011, **196**, 7323.
92 G. Tsekouras, D. Neagu and J. T. S. Irvine, *Energy Environ. Sci.*, 2013, **6**, 256.
93 S. Hui and A. Petric, *Mater. Res. Bull.*, 2002, **37**, 1215.
94 K. B. Yoo and G. M. Choi, *ECS Trans.*, 2009, **25**, 2259.
95 X. Li, H. Zhao, N. Xu, X. Zhou, C. Zhang and N. Chen, *Int. J. Hydrogen Energy*, 2009, **34**, 6407.
96 S. H. Cui, J. H. Li, X. W. Zhou, G. Y. Wang, J. L. Luo, K. T. Chuang, Y. Bai and L. J. Qiao, *J. Mater. Chem. A*, 2013, **1**, 9689.
97 K. B. Yoo, B. H. Park and G. M. Choi, *Solid State Ionics*, 2012, **225**, 104.
98 F. Napolitano, D. G. Lamas, A. Soldati and A. Serquis, *Int. J. Hydrogen Energy*, 2012, **37**, 18302.
99 C. Arrivé, T. Delahaye, O. Joubert and G. Gauthier, *J. Power Sources*, 2013, **223**, 341.
100 J. C. Ruiz-Morales, J. Canales-Vázquez, C. Savaniu, D. Marrero-López, W. Zhou and J. T. S. Irvine, *Nature*, 2006, **439**, 568.

101 D. Neagu and J. T. S. Irvine, *Chem. Mater.*, 2011, **23**, 1607.
102 C. Hatchwell, N. Bonanos and M. Mogensen, *Solid State Ionics*, 2004, **167**, 349.
103 X. Li, H. Zhao, F. Gao, N. Chen and N. Xu, *Electrochem. Commun.*, 2008, **10**, 1567.
104 R. J. Gorte and J. M. Vohs, *Curr. Opin. Colloid Interface Sci.*, 2009, **14**, 236.
105 H. Y. Chang, S. H. Wang, Y. M. Wang, C. W. Lai, C. H. Lin and S. Y. Cheng, *Int. J. Hydrogen Energy*, 2012, **37**, 7771.
106 X. Sun, S. Wang, Z. Wang, X. Ye, T. Wen and F. Huang, *J. Power Sources*, 2008, **183**, 114.
107 M. D. Gross, J. M. Vohs and R. J. Gorte, *Electrochem. Solid-State Lett.*, 2007, **10**, B65.
108 G. Kim, M. D. Gross, W. Wang, J. M. Vohs and R. J. Gorte, *J. Electrochem. Soc.*, 2008, **155**, B360.
109 T. Kolodiazhnyi and A. Petric, *J. Electroceram.*, 2005, **15**, 5.
110 S. Lee, G. Kim, J. M. Vohs and R. J. Gorte, *J. Electrochem. Soc.*, 2008, **155**, B1179.
111 M. A. Buccheri and J. M. Hill, *J. Electrochem. Soc.*, 2012, **159**, B361.
112 C. D. Savaniu and J. S. Irvine, *J. Mater. Chem.*, 2009, **19**, 8119.
113 K. B. Yoo and G. M. Choi, *Solid State Ionics*, 2009, **18**, 867.
114 K. B. Yoo and G. M. Choi, *Solid State Ionics*, 2011, **192**, 515.
115 C. D. Savaniu, D. N. Miller and J. T. S. Irvine, *J. Am. Ceram. Soc.*, 2013, **96**, 1718.
116 C. D. Savaniu and J. T. S. Irvine, *Solid State Ionics*, 2011, **192**, 491.
117 M. Roushanafshar, J. L. Luo, K. T. Chuang and A. R. Sanger, *ECS Trans.*, 2011, **35**, 2799.
118 M. Roushanafshar, J. L. Luo, A. L. Vincent, K. T. Chuang and A. R. Sanger, *Int. J. Hydrogen Energy*, 2012, **37**, 7762.
119 M. R. Pillai, I. Kim, D. M. Bierschenk and S. A. Barnett, *J. Power Sources*, 2008, **185**, 1086.
120 X. H. Zhang, J. Zhang, C. Yuan and E. J. Liang, *Adv. Mater. Res.*, 2012, **347–353**, 3325.
121 W. Kobsiriphat, B. D. Madsen, Y. Wang, M. Shah, L. D. Marks and S. A. Barnett, *J. Electrochem. Soc.*, 2010, **157**, B279.
122 B. D. Madsen, W. Kobsiriphat, Y. Wang, L. D. Marks and S. A. Barnett, *J. Power Sources*, 2007, **166**, 64.
123 L. Adijanto, V. B. Padmannabhan, R. Küngas, R. J. Gorte and J. M. Vohs, *J. Mater. Chem.*, 2012, **22**, 11396.
124 D. Neagu, G. Tsekouras, D. N. Miller, H. Ménard and J. T. S. Irvine, *Nat. Chem.*, 2013, 17731, DOI: 10.1038/NCHEM.
125 S. P. Jiang, *Int. J. Hydrogen Energy*, 2012, **37**, 449.
126 H. Birol, C. R. Rambo, M. Guiotoku and D. Hotza, *RSC Adv.*, 2013, **3**, 2873.
127 R. Pelosato, C. Cristiani, G. Dotelli, M. Mariani, A. Donazzi and I. N. Sora, *Int. J. Hydrogen Energy*, 2013, **38**, 480.
128 H. Okuyucu, H. Cinici and T. Konak, *Ceram. Int.*, 2013, **39**, 903.
129 X. Zhou, D. Zhan, C. Cong, G. Guo, L. Wang and K. Zhang, *J. Mater. Sci.*, 2005, **40**, 2577.
130 Y. J. Zhong, J. T. Li, Z. G. Wu, X. D. Guo, B. H. Zhong and S. G. Sun, *J. Power Sources*, 2013, **234**, 217.
131 M. Liu, P. He, J. L. Luo, A. R. Sanger and K. T. Chuang, *J. Power Sources*, 2001, **94**, 20.
132 P. He, M. Liu, J. L. Luo, A. R. Sanger and K. T. Chuang, *J. Electrochem. Soc.*, 2002, **149**, A808.
133 V. Vorontsov, W. An, J. L. Luo, A. R. Sanger and K. T. Chuang, *J. Power Sources*, 2008, **179**, 9.
134 X. Zhu, Q. Zhong, D. Xu, H. Yan and W. Tan, *J. Alloys Compd.*, 2013, **555**, 169.
135 D. Xu, Y. Bu, W. Tan and Q. Zhong, *Appl. Surf. Sci.*, 2013, **268**, 246.
136 R. Mukundan, E. L. Brosha and F. H. Garzon, *Electrochem. Solid-State Lett.*, 2004, **7**, A5.
137 A. L. Vincent, J. L. Luo, K. T. Chuang and A. R. Sanger, *Appl. Catal., B*, 2011, **106**, 114.
138 J. D. Kirtley, D. M. Halat, M. D. McIntyre, B. C. Eigenbrodt and R. A. Walker, *Anal. Chem.*, 2012, **84**, 9745.
139 A. K. Huber, M. Falk, M. Rohnke, B. Luerβen, L. Gregoratti, M. Amati and J. Janek, *Phys. Chem. Chem. Phys.*, 2012, **14**, 751.